Applied Energy 298 (2021) 117187

Contents lists available at ScienceDirect

Applied Energy

journal homepage: www.elsevier.com/locate/apenergy

Teaching-learning self-study approach for optimal retrofitting of dual mixed refrigerant LNG process: Energy and exergy perspective

Muhammad Abdul Qyyum [a,1], Faisal Ahmed [b,1], Alam Nawaz [a], Tianbiao He [c,*], Moonyong Lee [a,*]

[a] School of Chemical Engineering, Yeungnam University, Gyeongsan 712-749, Republic of Korea
[b] Department of Chemical Engineering, COMSATS University Islamabad (CUI), Lahore Campus, Defense Road, Off Raiwind Road, Lahore, Pakistan
[c] Department of Gas Engineering, College of Pipeline and Civil Engineering, China University of Petroleum (East China), Qingdao 266580, China

HIGHLIGHTS

- Dual mixed refrigerant LNG process is improved successfully.
- Joule-Thomson expansion device is replaced with hydraulic turbine.
- Teaching-learning self-study optimization algorithm is adopted.
- The DMR process gives LNG at the expense of 0.255 kWh/kg-LNG.
- Exergy efficiency of the LNG process is increased by 13.37% exergy.

GRAPHICAL ABSTRACT

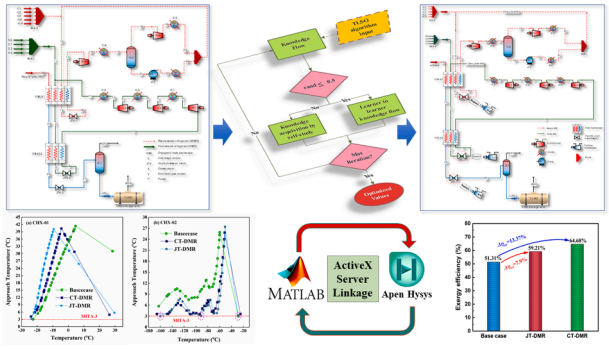

ARTICLE INFO

Keywords:
Natural gas liquefaction
DMR process
Teaching-learning optimization
Energy efficiency
Figure of merit
Cryogenic liquid turbine

ABSTRACT

This study unfolds the advanced process configuration modification in the evolution of a dual mixed refrigerant (DMR) process for natural gas liquefaction, followed by its optimization through a unique approach i.e., teaching–learning self-study optimization (TLSO). The DMR process is improved by replacing Joule Thomson valves with the isentropic cryogenic turbines. To ensure the maximum possible thermodynamic performance of the retrofitted DMR process, the TLSO paradigm is used and evaluated. The energy, exergy, coefficient of performance, and figure of merit are determined and compared with conventional bench-scale DMR process to find the performance improvement opportunities in the proposed cryogenic turbine-retrofitted DMR process. The performance analysis revealed that the proposed optimal retrofitted DMR process could produce LNG using 28.57% less energy than the base case. The detailed thermodynamic evaluation revealed that the proposed DMR process has 64.68% exergy efficiency, 2.42 coefficient of performance, and 41.6% figure of merit, which are 13.37%, 19%, and 11.9%, higher than the conventional DMR process, respectively. This study would significantly help process engineers overcome the challenges of relating energy efficiency of the LNG plants for both onshore and offshore applications.

* Corresponding authors.
E-mail addresses: hetianbiao@upc.edu.cn (T. He), mynlee@yu.ac.kr (M. Lee).
[1] These two authors contributed equally.

https://doi.org/10.1016/j.apenergy.2021.117187
Received 23 February 2021; Received in revised form 6 May 2021; Accepted 25 May 2021

1. Introduction

Natural gas has been one of the spotlights in the global energy market because of its relatively clean product after combustion [1]. Liquefied natural gas (LNG) is one of the dominant technologies for natural gas transportation and storage, which cools natural gas to −162 °C at atmospheric pressure and reduces its volume to 1/600~1/625 [2].

Natural gas liquefaction processes are energy-intensive [3] and cost-concentrated due to cryogenic working conditions [4]. The three typical types of natural gas liquefaction processes are mixed refrigerant process [5], cascade process [6], and nitrogen expansion process [7]. Many studies have been conducted on these three processes to reduce energy consumption [8] and equipment cost [9]. The mixed refrigerant process has been widely adopted as it has low energy consumption and relatively simple process configuration [10]. However, the complex nonlinear thermodynamic interaction increases the difficulty of obtaining optimal mixed refrigerant composition and other operational parameters [11]. The most prominent process for the base-load LNG plant is the propane precooled mixed refrigerant process (APCI-C3MR) [12] developed by Air Product [13]. However, the propane precooled refrigeration cycle has restricted the improvement of the single-train liquefaction capacity [14].

The dual mixed refrigerant (DMR) process consists of two independent mixed refrigerant cycles that can increase the liquefaction capacity and reduce energy consumption [15]. In the DMR process, one cycle utilizes high boiling point components in the precooling cycle, whereas the other cycle adopts low boiling point components to liquefy and subcool natural gas [16]. Many studies have investigated the effects of key parameters on the performance of the DMR process. Vatani et al. [17] analyzed the exergy destruction distribution of the DMR process by splitting the exergy destruction into avoidable or unavoidable and endogenous or exogenous. The results implied that the compressor in the cold mixed refrigerant cycle performed the highest unavoidable endogenous exergy destruction in the DMR process. Ma et al. [18] explored the effects of the precooling temperature and mixed refrigerant compositions on the energy consumption of the DMR process. The optimal components for warm and cold mixed refrigerants were ethane/pentane and methane/propane/nitrogen, respectively. Qyyum et al. [19] investigated the influences of the uncertain disturbances of the DMR process on the minimum internal temperature approach (MITA). The study results indicated that the cold mixed refrigerant compositions affected the MITA during the warm mixed refrigerant cycle.

Dynamic simulation and experimental study on DMR process also provide an insight of the practical operation characteristic. Michelsen et al. [20] proposed a dynamic model of the DMR process to investigate the control characteristics. They noted that the mixed refrigerant flowing behavior could impact the heat transfer curves in the cold box. Husnil and Lee [21] built a rigorous dynamic model of the DMR process to examine the possible control variables. It was noted that the mixed refrigerant flow ratio of the precooling and subcooling cycles was the optimal control variable to keep the process stable. Then, Sun et al. [22] experimentally studied the pressure drop and heat transfer performance [23] in a spiral-wound heat exchanger of the DMR process with sloshing. They found that the pressure drop of the vapor refrigerant was significantly influenced. Moreover, the heat transfer coefficient decreased by 50% under the sloshing conditions.

Modifying the configuration of the DMR process is another approach that could improve its performance. Hwang et al. [24] presented a synthesis study to design the DMR process for LNG-FPSO based on several principles. Their optimal design reduced 7.45% of the overall power consumption compared to the conventional DMR process. Vatani et al. [25] integrated the DMR process with the NGL recovery process to diminish the specific power and improve the economic performance. The integrated process was optimized in several segments using stochastic methods to simplify the optimization procedure. The optimized results indicated 0.414 kWh/kg of specific power and 93% purity of the ethane produced. Notably, retrofitting of the DMR process may improve the energy performance. However, the drawback of retrofitting could increase the process complexity.

Several optimization studies have been conducted to reduce the energy consumption of the DMR process by optimizing the mixed refrigerant compositions in the two cycles, as shown in Table 1.

According to the literature review, it can be seen that modifying the DMR process configuration and adopting optimization algorithms are the main methods to reduce energy consumption. A hydraulic turbine is considered a good option for replacing the throttling valve in the DMR process to recover the expansion power [31], which can reduce the overall energy consumption significantly. However, adopting hydraulic turbine in the DMR process has not been reported in the open literature yet. Moreover, widely utilized optimization algorithm, GA and PSO, are sometimes easily stuck in the local optima because of the complex nonlinear interaction between the decision variables and the objective function [32]. Thus, it calls for advanced optimization algorithms to further reduce the energy consumption of the DMR process. To address these research gaps, this paper first presents a retrofitting of the DMR process by introducing hydraulic turbines to replace the JT valves in cold and warm refrigerant cycles. Further, the teaching–learning self-study optimization (TLSO) algorithm, which is a fast-converging algorithm with respect to the average fitness of the population with less probability of getting stuck in local optima, is adopted to lower the energy consumption of the process. The results were compared with the traditional DMR process, and the performance of retrofitting and the TLSO algorithm were validated. The TLSO algorithm can be applied to other processes to achieve global optima. This study brings some insights into how to retrofit the DMR process and adopt advanced optimization algorithm to improve the thermodynamic efficiency.

2. Conventional and retrofitted DMR processes: Description and simulation

2.1. Conventional dual mixed refrigerant process description

The flow diagram of the conventional DMR process is shown in Fig. 1. The feed natural gas was precooled in CHX-01 by the warm mixed refrigerant (WMR) cycle and then liquefied and subcooled in CHX-02 by the cold mixed refrigerant (CMR) cycle. Further, it went through the JT valve (JTV-3) to reduce its pressure to LNG storage pressure and entered

Table 1
Summary of optimization techniques on the DMR process.

Studies	Optimization algorithm	Key findings
Hwang et al. [26]	GA combined with sequential quadratic programming	1.2% reduction in power consumption
Khan et al. [27]	The elitist GA and box methodology	15% and 36% of UA and specific energy consumption savings, respectively
Lee and Moon [28]	Successive reduced quadratic programming (SRQPD)	22.5% profit increase
Vikse et al. [29]	Primal-dual interior-point optimizer	14.4% energy saving
Qyyum et al. [30]	Invasive-weed optimization algorithm	16.2% compression power saving

the LNG tank for storage.

The WMR consisting of methane, ethane, propane, i-butane, and n-butane were pressurized by the compressor (K-4) to a middle pressure. Then, some of the high-boiling-point components in the WMR were condensed after passing through the water cooler. The vapor and liquid mixed refrigerant were further compressed by the compressor (K-5) and pump (P-1), respectively. Subsequently, the mixed refrigerant was pre-cooled to around −24 °C in CHX-01 and generated the refrigeration capacity for CHX-01 through the JT valve (JTV-1). The CMR comprising methane, ethane, propane, and nitrogen was pressurized by a three-stage compressor with intercoolers. The high-pressure CMR was cooled in CHX-01 and CHX-02 to −157.1 °C. The pressure was reduced to 1.5 bar through JT valve resulting a vapor–liquid mixture (around 90% liquid fraction) to enhance the cooling capacity of CHX-02 for liquefaction and subcooling of natural gas. Moreover, to reproduce the studied DMR LNG processes (base case, JT-DMR, and CT-DMR), all important information (such as temperature, pressure, flowrate, enthalpy, and exergy) associated with each stream are given as Section 2 in the *Supporting Information*.

2.2. Cryogenic turbine-retrofitted dual mixed refrigerant process

Fig. 2 illustrates the retrofitted DMR process by utilizing a cryogenic turbine (CT) to replace JT valves. The remaining process was the same as the conventional DMR process except for the three JT valves used for natural gas, WMR, and CMR throttling. The isentropic expansion that occurred in the CT could recover the expansion power and obtain higher temperature drops than the isenthalpic expansion that occurred in the JT valve. According to the JT coefficient (μ_{JT}) and isentropic expansion coefficient (μ_S) defined in Eqs. (1) and (2), the temperature drop obtained by the isentropic expansion based on the same pressure drop was consistently larger than that obtained by JT throttling. Thus, to produce the same amount of cooling capacity, the retrofitted DMR process could use a mixed refrigerant with a reduced flow rate or lower pressure before entering the CT that could result in lower energy consumption and higher thermodynamic efficiency.

$$\mu_{JT} = \left(\frac{\partial T}{\partial P}\right)_h = \frac{1}{C_p}\left[T\left(\frac{\partial v}{\partial T}\right)_P - v\right] \tag{1}$$

$$\mu_S = \left(\frac{\partial T}{\partial P}\right)_s = \frac{T}{C_p}\left(\frac{\partial v}{\partial T}\right)_P \tag{2}$$

2.3. Process simulation

The conventional and retrofitted DMR processes were simulated using well-known commercial simulator Aspen HYSYS®. The Peng–Robinson equation of state [33] was used to calculate the thermodynamic properties. The inlet temperature, pressure, and mass flow rate of the feed natural gas were 25 °C, 5500 kPa, and 124,700 kg/h, respectively. The composition of the feed natural gas is given in Table 2.

The major assumptions that were made to simulate the DMR process are:

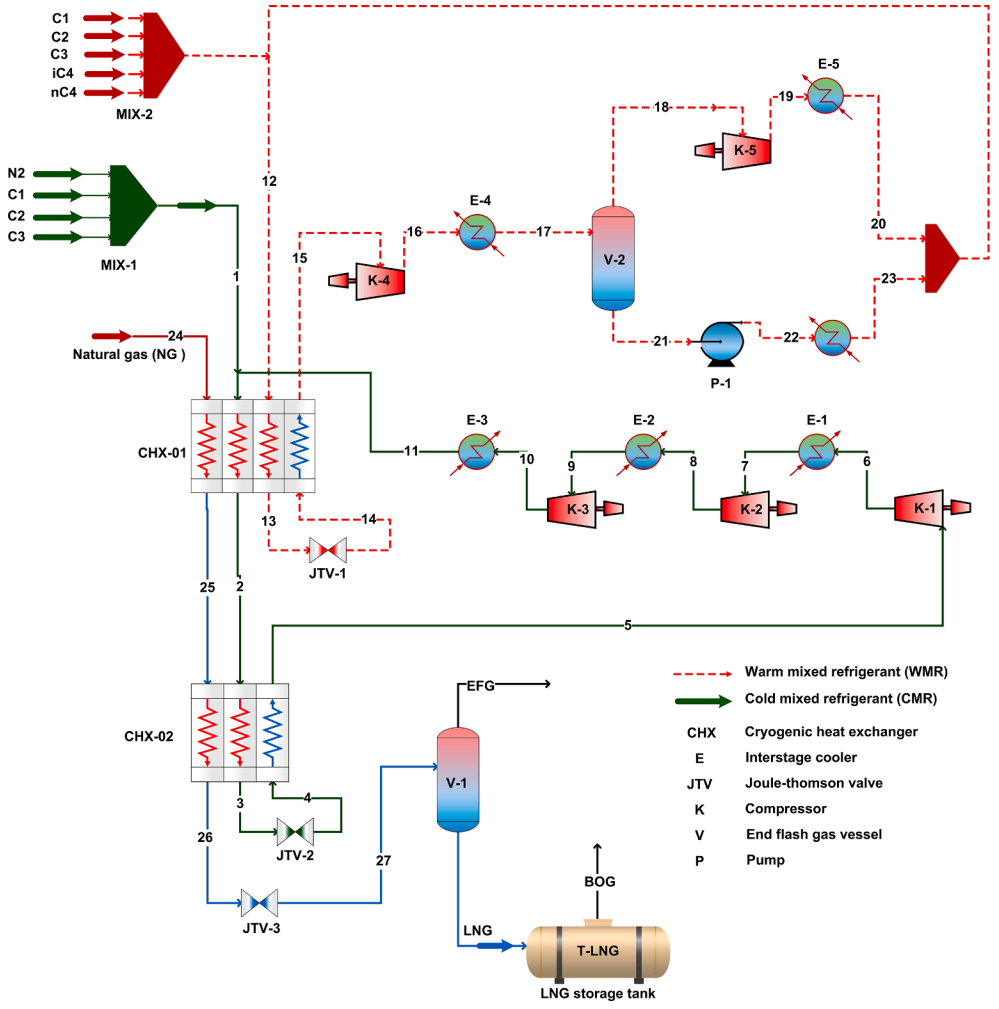

Fig. 1. Flow diagram of the conventional DMR process.

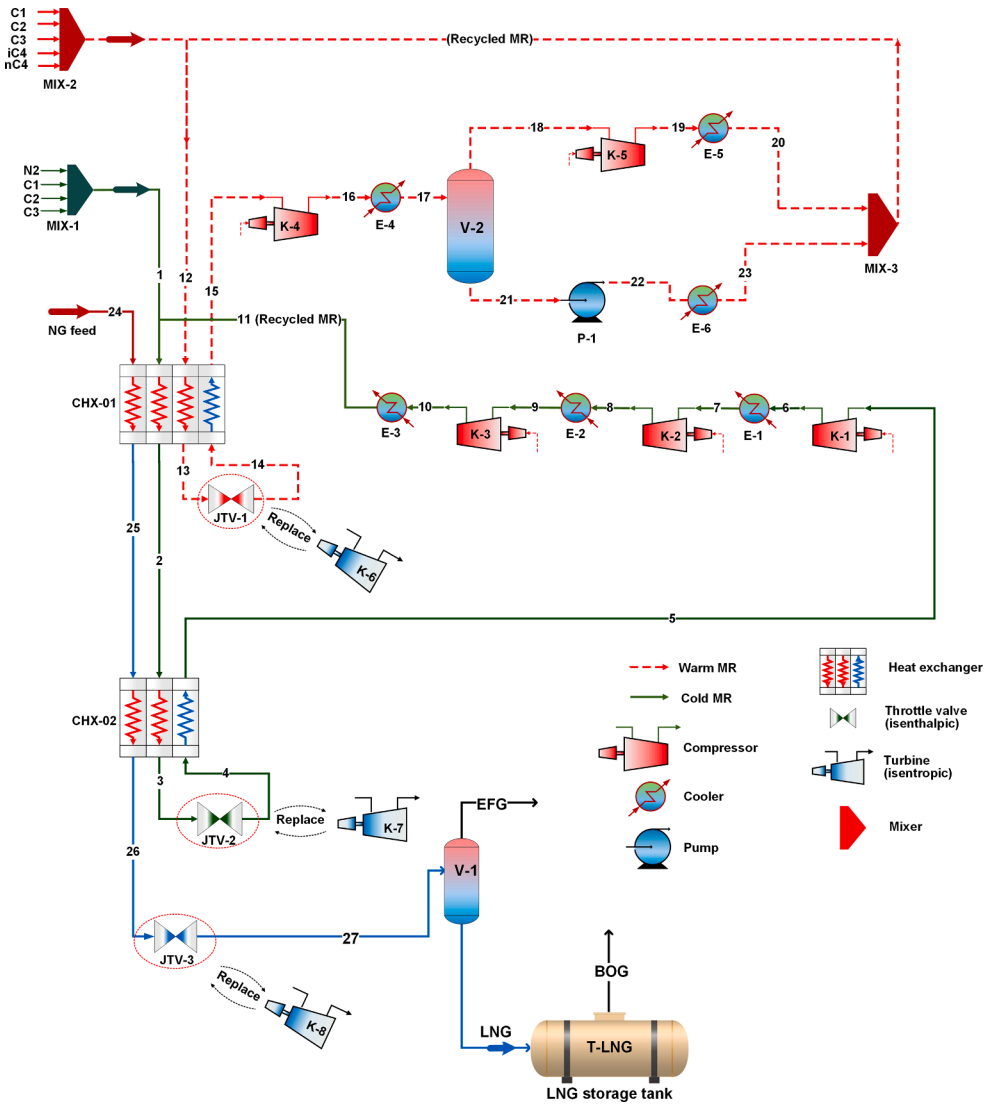

Fig. 2. Flow diagram of the retrofitted DMR process.

- The process was in a steady-state.
- The LNG storage conditions were 110 kPa and −160 °C with the pressure a little bit higher than the atmospheric pressure.
- The adiabatic efficiency of the compressor, pump, and turbine were 75%, 75%, and 90%, respectively.
- The MITA of the cryogenic heat exchanger was 3 °C, which gave an enough heat transfer driving force without increasing the heat transfer area significantly.
- The pressure drops of the natural gas, WMR stream, and CMR stream in the cryogenic heat exchanger were 100, 50, and 10 kPa, respectively.

Table 2
Molar Fraction of the feed natural gas.

Component	Molar fraction
CH_4	0.8722
C_2H_6	0.0669
C_3H_8	0.0349
i-C_4H_{10}	0.0060
n-C_4H_{10}	0.0090
i-C_5H_{12}	0.0030
n-C_5H_{12}	0.0020
n-C_6H_{14}	0.0010
N_2	0.0050

- The pressure drop of the water cooler was 50 kPa.

3. Teaching-learning self-study approach for optimization

Since the advent of computers, solving optimization problems using the evolutionary algorithm (EA) has become an important application area and is currently one of the hot topics of interest [34]. The EA has shown remarkable realization and proven to be a rigorous technique for solving complex real-world engineering problems over the decades [35]. By contrast, much has not been done for chemical processes using EA as an optimization tool [36]. However, recently, researchers have focused on solving various problems related to chemical processes utilizing EAs [37].

EAs are usually based on social phenomena and real-life examples, for example, ant colony optimization (ACO) [38] and PSO [39]. Teaching and learning in an educational environment as a social phenomenon may be modeled as an EA for optimization. An EA based on the social phenomenon of teaching and learning was first developed by Rao et al. [40] named teaching–learning based optimization (TLBO). TLBO was then ameliorated by Li et al. and named ameliorated teaching–learning based optimization (ATLBO) [41]. In a learning environment, apart from teaching, there exists a natural phenomenon that allows learners to gain knowledge utilizing resources available such as

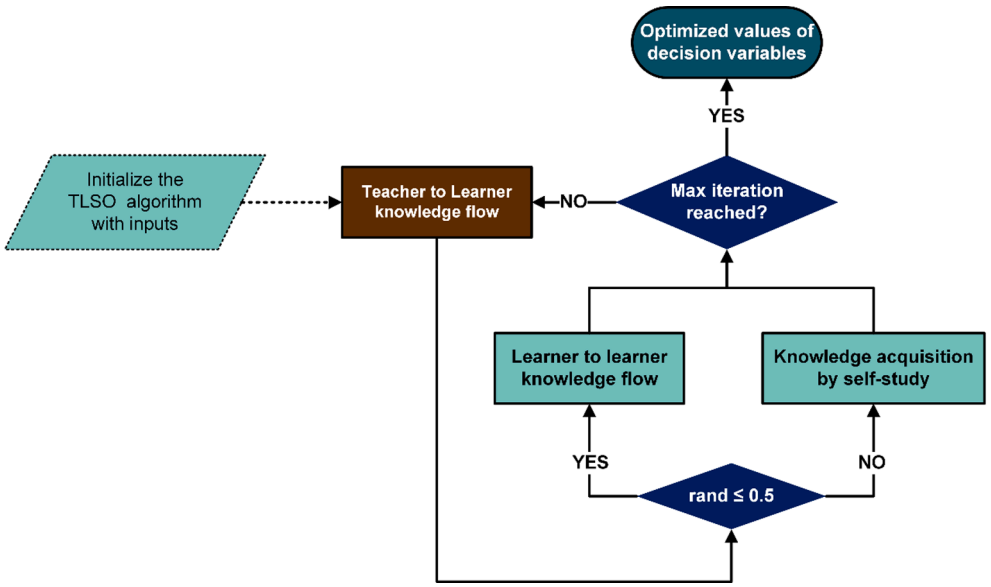

Fig. 3. Simplified schematic of TLSO algorithm.

libraries and internet. This concept has been incorporated by Ahmed et al., and the algorithm is known as teaching–learning self-study optimization (TLSO) [42]. A brief description of the TLSO algorithm is as follows:

The social phenomenon of the TLSO algorithm is based on three main modes.

(1) Teacher to learner knowledge flow: The most knowledgeable and learned person in a class is considered a teacher, whose responsibility is to share knowledge with the learners and inspire them.

(2) Learner to learner knowledge flow: In a classroom environment, learners interact and share knowledge. More knowledgeable learners share their knowledge with lesser knowledgeable learners.

(3) Knowledge acquisition by Self-Study: Some learners may prefer self-study over interaction with other learners. These learners study articles, patents, books and various theses to gain knowledge.

The two vital components of a robust optimization algorithm are intensification and diversification. Further, a balanced adjustment between intensification and diversification is crucial in an optimization algorithm. The TLSO focuses on both vital concepts. In this case, the intensification is assimilated by the teacher to learner knowledge flow mode and the learner to learner knowledge flow mode. These two phenomena, in general, accelerate convergence towards the destination. The third mode, knowledge acquisition by self-study, covers the diversification phenomenon by allowing learners to search for information by themselves minimizing the possibility of divergence at local minima. As a result, it increases the ability of the algorithm to obtain global minimum. The basic flowchart of the TLSO algorithm is shown in Fig. 3.

4. Optimization of the dual mixed refrigerant process

This study aimed to achieve the minimum SEC in the DMR process. Thus, the objective function of TLSO optimization, used for this study, was:

$$f(X) = Min.\left(\frac{\dot{W}_t}{\dot{m}_{LNG}}\right) \tag{3}$$

where X is a vector containing the decision variables for optimization, $f(X)$ represents SEC, $\dot{W}_t$ is the total energy consumption of the DMR process and $\dot{m}_{LNG}$ is the mass flow rate of LNG.

In the case of the DMR process, the decision variables are the mixed refrigerant compositions, evaporation, and condensation pressures of the warm and cold mixed refrigerant cycles. Further, the precooled temperature (stream 13) is a key variable for the DMR process because it determines the heat load distribution in CHX-01 and CHX-02. Thus, the precooled temperature is also included in the decision variables. The lower and upper bounds of the decision variables are listed in Table 3. X can be expressed in Eq. (4):

$$\mathrm{X}=\left[\dot{m}^{c}_{CH_4},\dot{m}^{c}_{C_2H_6},\dot{m}^{c}_{C_3H_8},\dot{m}^{c}_{N_2},P_4,P_{10},\dot{m}^{w}_{C_2H_6},\dot{m}^{w}_{C_3H_8},\dot{m}^{w}_{iC_4H_{10}},\dot{m}^{w}_{nC_4H_{10}},P_{13},P_{20},T_{13}\right] \tag{4}$$

where the superscripts c and w denote the cold and warm mixed refrigerant cycles, respectively.

The constraint is necessary to ensure that the search direction is correct during the optimization procedure. In this study, MITA of CHX-01 and CHX-02 are selected as the constraints, which should be larger than 3 °C to maintain a sufficient heat transfer driving force between the hot and cold streams.

4.1. Teacher to learner knowledge flow

For any iteration a (number of iterations, $a = 1, 2, \ldots n$), there are $s = 13$ number of decision variables (courses in TLSO terminology, $m = 1,2, \cdots s$) and $k = 50$ population size (number of learners, $i = 1,2, \cdots k$).

The TLSO algorithm initializes by assigning random values of deci-

Table 3
Lower and upper bounds of the decision variables.

Variables	Lower bounds	Upper bounds
$\dot{m}^{c}_{CH_4}$ (kg/s)	8.5	15.5
$\dot{m}^{c}_{C_2H_6}$ (kg/s)	14.5	20
$\dot{m}^{c}_{C_3H_8}$ (kg/s)	30	45
$\dot{m}^{c}_{N_2}$ (kg/s)	2.5	6.5
P_4 (kPa)	110	450
P_{10} (kPa)	3000	6000
$\dot{m}^{w}_{C_2H_6}$ (kg/s)	0.5	3.5
$\dot{m}^{w}_{C_3H_8}$ (kg/s)	30	50
$\dot{m}^{w}_{iC_4H_{10}}$ (kg/s)	5	20
$\dot{m}^{w}_{nC_4H_{10}}$ (kg/s)	5	20
P_{13} (kPa)	110	350
P_{20} (kPa)	800	2500
T_{13} (°C)	−30	−10

sion variables to learners within their bounds. It forms a vector of decision variable values (X) associated with each learner. The specific energy consumption is calculated using the assigned values of decision variables. To handle the constraints, a penalty is imposed on the specific energy consumption of the learner whose solution is infeasible, that is when constraints are not satisfied. The constraint handling procedure can be found in detail in other research works [43].

The vector that gives the lowest SEC (best fitness value) is the vector associated with the teacher, which is:

$$X_{teacher} = X_{\min,f(X)} = X_{min.SEC} \tag{5}$$

The teacher must uplift the learners with worse values of decision variables associated with higher SEC by giving more attention to them than those with lower SEC. Hence, during iteration, the learner with worse values of decision variables will take a large step, but the learner with better values of decision variables will take a small step toward the teacher to modify or update his/her values. For a particular learner, the modified decision variable values depend on his/her old decision variable values and the difference between $X_{teacher}$ and the mean of the values obtained by other learners (M_i). It can be expressed as follows [41]:

$$X_{mod,i} = \Omega_i X_{old,i} + \Gamma_i (X_{teacher} - T_F M_i) \tag{6}$$

where $X_{old,i}$ and $X_{mod,i}$ are the i^{th} learner's decision variable values before and after learning from the teacher, respectively.

T_F is the teaching factor that can take the value of either 1 or 2, which is decided by $T_F = \text{round}[1 + rand(0,1)(2-1)]$. The value of T_F decides the value of the mean to be used in the Eq. (2). Ω_i is the inertia weight that gives weight to the previous decision variable values and maintains a well-adjusted impact of historical influence to the modified decision variable values. Γ_i controls the step size of the difference ($X_{teacher} - T_F M_i$) and is called the acceleration coefficient. Γ_i can take values from 0 to 1. Ω_i and Γ_i are represented as:

$$\Omega_i = 1/\left(1 + \exp\left(-\frac{SEC_i}{SEC_{teacher}}\right)^{iter}\right) \tag{7}$$

$$\Gamma_i = 1/\left(1 + \exp\left(-\frac{SEC_i}{SEC_{teacher}}\right) iter\right) \tag{8}$$

where SEC_i is the specific energy consumption associated with the i^{th} learner, and $SEC_{teacher}$ is the specific energy consumption associated with the teacher in the first iteration.

After the modification of the values of decision variables of all the learners is completed using Eq. (2), the SECs of all learners are computed again while imposing penalties on the infeasible solutions. The modified values of decision variables and SECs are concatenated with the previous values of the decision variables and SECs, respectively. Learners with the lowest SEC compared to other learners in a class are considered elite. The selection of elite learners in the subsequent steps is called the elitist strategy. Finally, the SECs are sorted in ascending order, and their values of decision variables are assigned accordingly. Eventually, after the elite learners are selected, the flow of algorithm moves towards the next section of the algorithm.

4.2. Learner to learner knowledge flow

The learner to learner knowledge flow mode allows the learners to interact with each other such that an exchange of knowledge between learners with higher knowledge and other learners takes place. This process can be described as follows:

In the i^{th} sub-iteration, for a learner with values of decision variables X_i, another learner with values of decision variables X_j is randomly selected, where $i \neq j$. The learner with the values of decision variables X_i modifies his/her values of decision variables according to the randomly assigned learner as follows:

$$X_{\text{mod},i} = \begin{cases} X_{\text{old},i} + r_i\left(X_i - X_j\right) iff\left(X_i\right) < f\left(X_j\right) \\ X_{\text{old},i} + r_i\left(X_j - X_i\right) iff\left(X_i\right) \geq f\left(X_j\right) \end{cases} \tag{9}$$

where r_i is a uniformly distributed random number ranging from 0 to 1, which randomly adopts the step size of the difference. If $X_{\text{mod},i}$ gives lower SEC, it is accepted and the algorithm moves on.

4.3. Knowledge acquisition by self-study

As the teacher to learner and the learner to learner knowledge flow modes intensify the search convergence, knowledge acquisition by self-study mode allows diversification in the search space to minimize the risk of diverging at a local minimum. To inculcate diversification, TLSO introduces the diversification factor D as follows:

$$D_m = X_m^U - X_m^L \tag{10}$$

where D_m, X_m^U, and X_m^L are the min–max search space, upper bound, and lower bound of the m^{th} decision variable, respectively.

The algorithm of the learner to learner knowledge flow and knowledge acquisition by self-study with equal probability, can be described as:

if rand < 0.5

$$X_{\text{mod},i} = \begin{cases} X_{\text{old},i} + r_i\left(X_i - X_j\right) & if\ f\left(X_i\right) < f\left(X_j\right) \\ X_{\text{old},i} + r_i\left(X_j - X_i\right) & if\ f\left(X_i\right) \geqslant f\left(X_j\right) \end{cases}$$

otherwise

$$X_{\text{mod},i} = \begin{cases} X_{\text{old},i} - r_i D_m if\, r_i D_m < X_{\text{old},i} \\ X_{\text{old},i} + r_i D_m if\, r_i D_m = X_{\text{old},i} \\ r_i D_m - X_{\text{old},i} if\, r_i D_m > X_{\text{old},i} \end{cases} \tag{11}$$

where rand is a uniformly distributed random number ranging from 0 to 1.

After the decision variable values are modified and the values of SEC are computed for all learners with penalties where the solution is infeasible is completed, the elitist strategy, like that of the teacher to learner knowledge flow mode, is executed. The detailed flowchart of the TLSO algorithm is given in Fig. 4. Whereas, the Pseudocode of the TLSO algorithm is also given in section 1 of the *Supporting Information*.

5. Results and discussions: Process analysis

5.1. Parametric analysis

The DMR process optimized by knowledge-based optimization (KBO) is selected as the base case to illustrate the superiority of the TLSO on the optimization of the DMR process. The optimized decision variables and process performance are listed in Tables 4 and 5.

The SEC of the JT-DMR process optimized by TLSO is 0.288 kWh/kg, which is 19.32% lower than that of the base case as the suitable compositions of the warm and cold MR were obtained for the process. For the warm MR refrigeration cycle in the JT-DMR process, the total MR flow rate is 76.80 kg/s, which is 3.29% lower than the base case. The flow rates of ethane and i-butane reduce, while the flow rates of propane and n-butane increase. It indicates that the optimal mixed refrigerant prefers more high boiling point components rather than low boiling point components. Moreover, the pressure ratio is 6.45, which is 48.06% lower than the base case. Both these effects result in 19.82% energy saving when compared to the base case. These results indicate that the warm MR composition optimized by TLSO has a larger specific refrigeration capacity and consumes less energy to achieve the same precooling requirement. For the cold MR refrigeration cycle in the JT-DMR

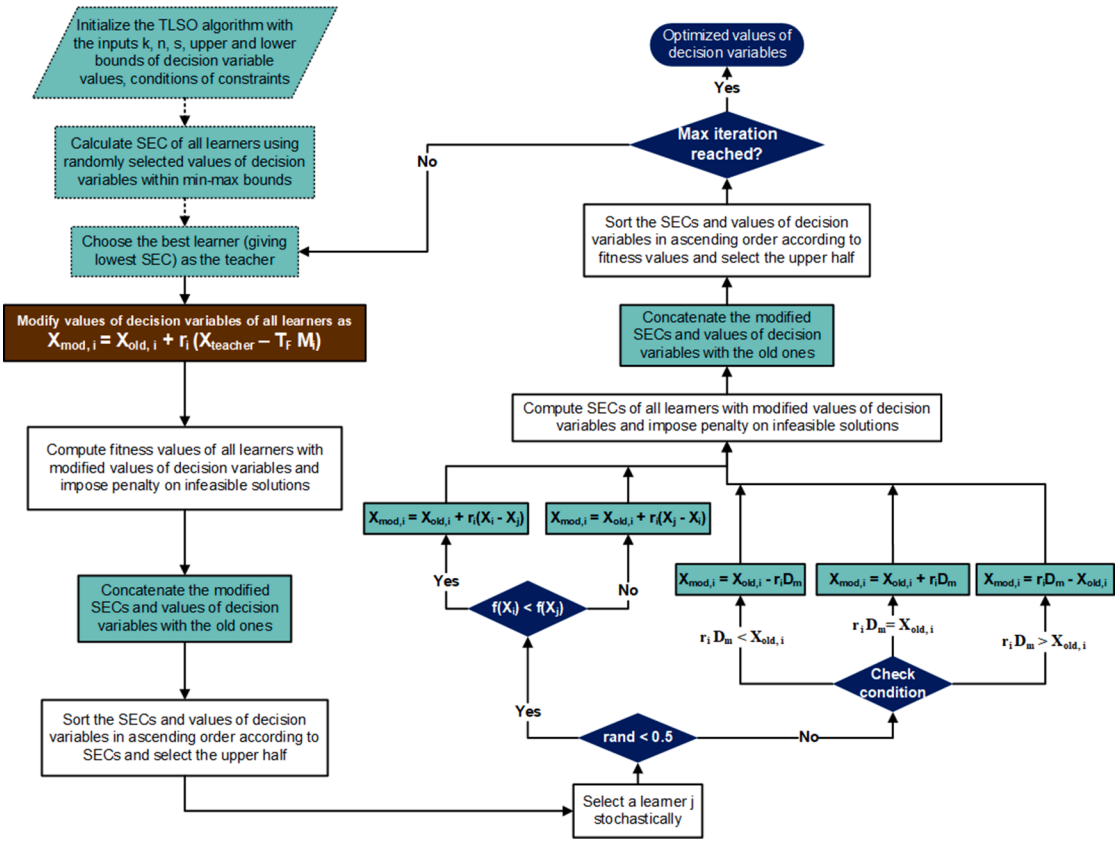

Fig. 4. Flowchart of TLSO algorithm for DMR process.

Table 4
Optimized decision variables of the base case, JT-DMR, and CT-DMR processes.

Parameters	Base case		JT-DMR		CT-DMR	
	Warm MR	Cold MR	Warm MR	Cold MR	Warm MR	Cold MR
$\dot{m}_{N_2}$ (kg/s)	–	6.10	–	4.76	–	2.68
$\dot{m}_{CH_4}$ (kg/s)	–	13.50	–	13.40	–	12.80
$\dot{m}_{C_2H_8}$ (kg/s)	2.12	18.80	1.95	18.10	2.73	19.16
$\dot{m}_{C_3H_8}$ (kg/s)	45.30	29.92	46.85	32.88	33.0	30.0
$\dot{m}_{iC_4H_{10}}$ (kg/s)	17.50	–	13.88	–	10.20	–
$\dot{m}_{iC_4H_{10}}$ (kg/s)	14.50	–	14.12	–	17.50	–
Total flow rate (kg/s)	79.42	68.32	76.80	69.14	63.43	64.64
MR low pressure (kPa)	153.0	140.0	155.0	200.0	200.0	220.0
MR high pressure (kPa)	1900.0	5700.0	1000.0	4360.0	1400.0	5180.0
Precooling temp. (°C)	−25.50		−25.72		−21.00	
$MITA_{CHX-01}$ (°C)	3.0		3.0		3.0	
$MITA_{CHX-02}$ (°C)	3.0		3.0		3.0	
SEC (kWh/kg-LNG)	0.357		0.288		0.255	
Energy savings (%)	–		19.32		28.57	

process, the total MR flow rate is 69.14 kg/s, which is 1.20% higher than the base case. The flow rate of propane increases from 29.92 to 32.88 kg/s, which is 9.89% higher than the base case. However, the flow rate of nitrogen, methane, and ethane reduce by 21.97%, 0.74%, and 3.72%,

Table 5
Compressor power consumptions and CT power generations of three cases.

Compressor/Turbine		Base case	JT-DMR	CT-DMR
Cold MR cycle	K-1 (kW)	8661.90	6951.30	6816.39
	K-2 (kW)	11474.64	9270.02	8756.60
	K-3 (kW)	9792.79	8018.79	7474.48
	K-7 (kW)[a]	–	–	446.22
	K-8 (kW)[b]	–	–	320.43
	Net power (kW)	*29929.33*	*24240.11*	*22280.82*
Warm MR cycle	K-4 (kW)	6308.79	4981.77	4224.21
	K-5 (kW)	6801.50	5529.67	4323.75
	K-6 (kW)[c]	–	–	103.59
	Net power (kW)	*13110.29*	*10511.44*	*8444.37*
	Total power (kW)	43039.63	34751.55	30725.18

[a] CMR turbine
[b] LNG turbine
[c] WMR turbine

respectively. Due to the large temperature difference at the hot end, increasing the flow rate of high boiling point component (propane) could eliminate the large exergy loss and thereby reduce the energy consumption. Moreover, the pressure ratio decreased significantly from 40.71 (base case) to 21.80 (JT-DMR).

The CT-DMR process showed 28.57% and 11.46% relative energy saving compared to the base case and JT-DMR process, respectively. The JT-DMR and CT-DMR processes are compared in detail to demonstrate the benefit of the CT-retrofitted DMR process. The total flow rate of the warm MR in the CT-DMR process was 63.43 kg/s indicating a 17.41% reduction when compared to the JT-DMR process. Most of the flow rate reduction is contributed by propane, which decreases from 46.85 kg/s to 33.00 kg/s. The pressure ratios of the two processes were remarkably close (6.45 for JT-DMR, 7.00 for CT-DMR), which led to a 19.66% power reduction in the warm MR refrigeration cycle. Further, the power

consumed by the warm MR in the CT-DMR process was 18.68% lower than the JT-DMR, even after excluding the power recovery by the CT (K-8). The cold MR in the CT-DMR process had a lower total flow rate and a higher pressure ratio than the JT-DMR process, which enhanced the power reduction by 8.08% in the cold MR refrigeration cycle. Notably, the flow rate of nitrogen, methane, and propane decrease, while that of ethane increases. This benefits the heat transfer performance in the range of −100 to −80 °C. Furthermore, the optimal mixed refrigerant by using CT is different from that with JT. This might be explained by the different thermodynamic process occurred in CT (isentropic) and JT (isenthalpic).

From the previous analysis, it can be observed that the JT-DMR process optimized by TLSO had a higher thermodynamic efficiency when compared to the base case optimized by KBO. Further, by replacing the JT valve with the CT, the specific energy consumption of the DMR process can be reduced with a much appropriate MR composition.

5.2. Composite curves analysis

Changes made to the system are irreversible due to intransigent environmental condition. Process irreversibility is mainly due to the gap between the cold and hot composite curve (CC), representing more work loss. Thus, the TLSO algorithm needs to reduce the irreversibility by minimizing the gap between cold and hot CCs while satisfying the MITA criteria. The CCs analysis plays a vital role in determining the feasibility of the optimization results and which area has participated in more work loss (increased NG liquefaction cost), which can be narrowed further by suitable tuning of the decision variables. In fact, for an energy-efficient process, each cold and hot CC of the natural gas and mixed refrigerant should be placed near the feasible MITA, that is, 3 °C. The approach temperature (TDCC) and heat flow (THCC) plot of the JT-DMR and CT-

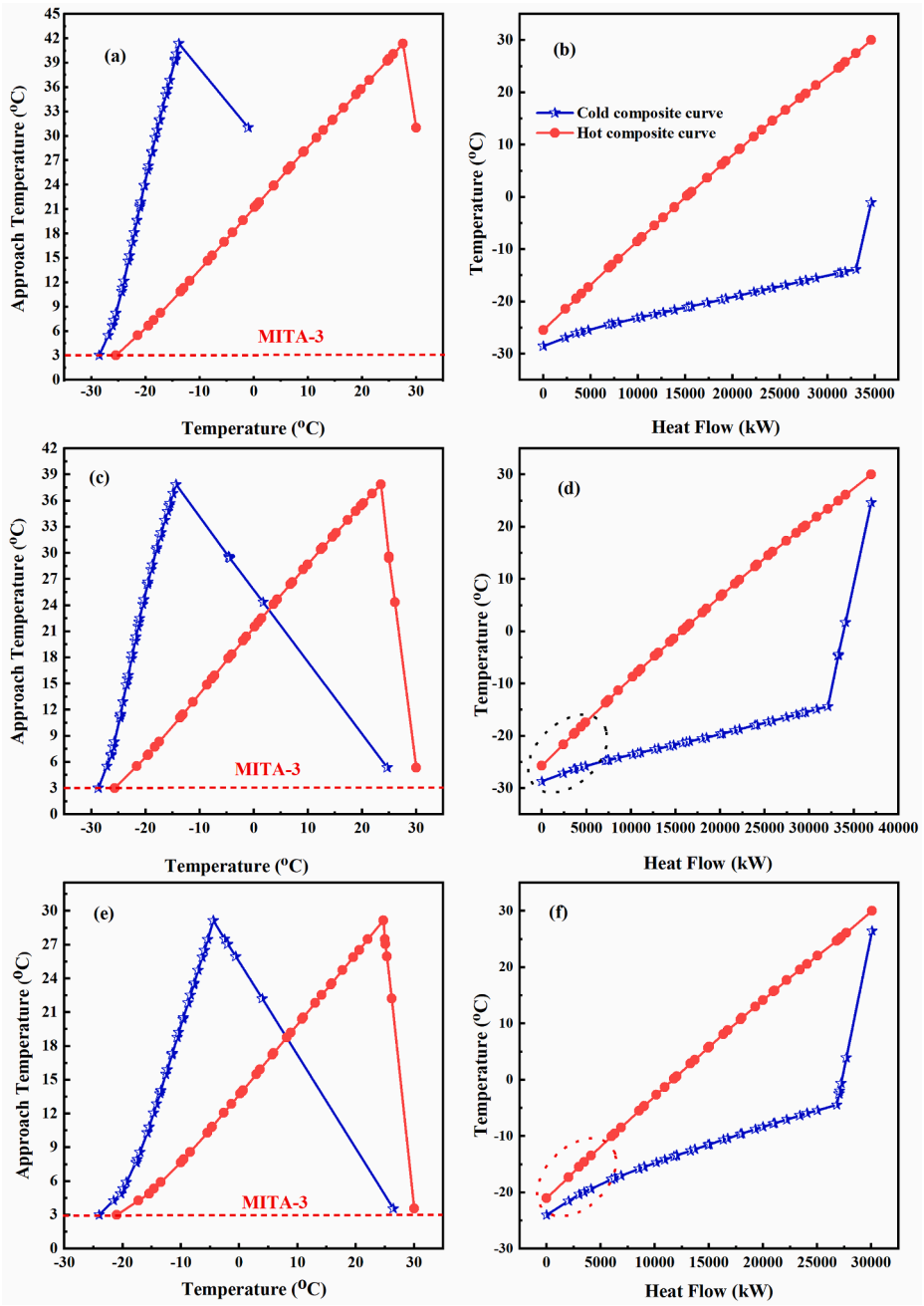

Fig. 5. TDCC and THCC composite curves for the heat exchanger CHX-1 (a, b) base case, (c, d) JT-DMR case and, (e, f) CT-DMR case.

DMR case for heat exchanger CHX-1 compared to the base case is presented in Fig. 5. For a clear understanding, a red dashed line is taken for the demonstration on TDCC plots (Fig. 5 (a, c, and e)), which indicates the MITA value (3 °C).

According to Fig. 5a and 5b, the cold and hot CCs of the TDCC region (at temperatures ranging from −30 to −10 °C) are less than 10 °C but immediately increase after 10 °C. Due to the MITA occurring at the cold end and the continuous evaporation of high boiling point components along the CHX-01, the slope of the cold composite curve is smaller than the hot composite curve leading to the increase of temperature difference. Nevertheless, for the JT-DMR case, the cold and hot CCs narrowed because of the presence of i-butane, as shown in Fig. 5c and 5d. Fig. 5a shows that the peak is significantly higher than that of Fig. 5c, which shows inefficient heat transfer in this region. By contrast, the large temperature difference (42 °C) of the base case was further reduced in the optimized JT-DMR and CT-DMR cases (Fig. 5e and 5f). Moreover, the CT-DMR case temperature difference curve showed better results compared to JT-DMR and the base case for heat exchanger CHX-1 and a smaller heat flow, as shown in Fig. 5.

The CCs and temperature difference for heat exchanger CHX-2 are illustrated in Fig. 6. The low temperature ranges from −160 to −60 °C of the TDCC region lies at MITA = 3 °C, as shown in Fig. 6e, but there is a high peak when the temperature is higher than −60 °C in comparison to Fig. 6a and 6c, which show inefficient heat transfer in Fig. 6a, c of JT-DMR, and base case, respectively, due to the presence of n-butane and i-butane. In Fig. 6e of the CT-DMR case, there is a maximum chance of improvement in the temperature range of −160 to −120 °C by suitable tuning of cold MR flow rates of N_2, C_1, C_2, and C_3. Nevertheless, a gap in the THCC region (see red circle) is narrowed, leading to low energy consumption in comparison to the JT-DMR and base case. In Fig. 6(d)

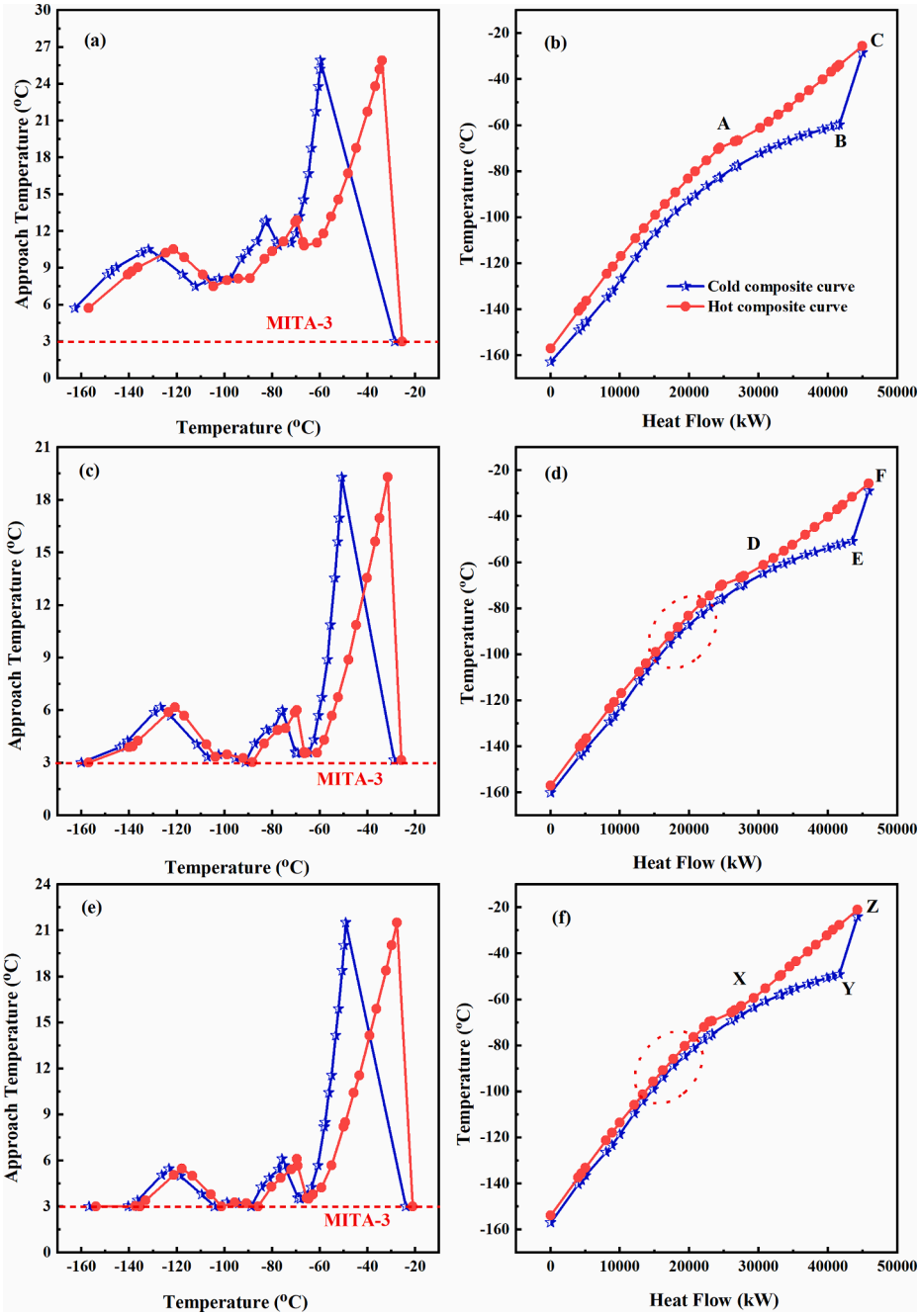

Fig. 6. TDCC and THCC composite curves for the heat exchanger CHX-2, (a, b) base case, (c, d) JT-DMR case and, (e, f) CT-DMR case.

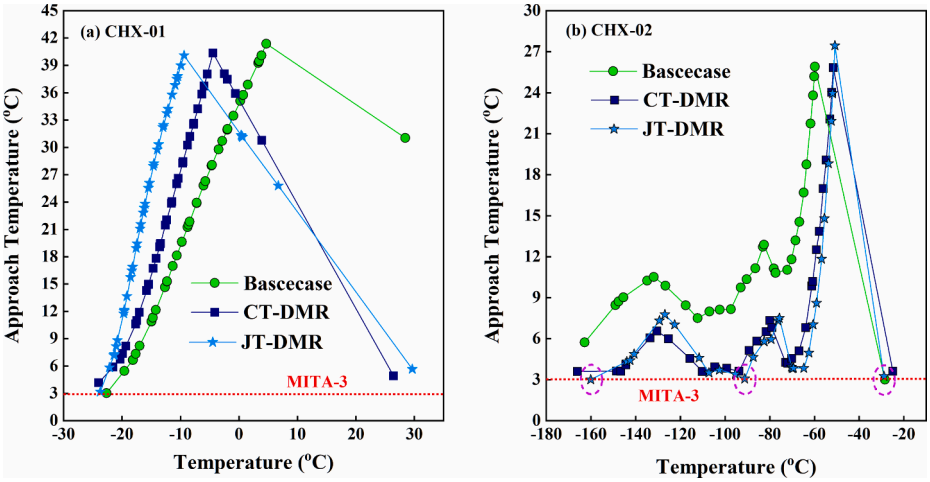

Fig. 7. TDCC comparison of three cases: (a) CHX-01, (b) CHX-02.

and (f), the triangle XYZ of the THCC region with minimized heat flow is significantly smaller than that of triangle DEF and ABC of JT-DMR and base case, respectively, which indicates that CT-DMR is an energy-efficient process compared to JT-DMR and the base case.

To demonstrate the improvement by process retrofitting and TLSO, TDCCs in CHX-01 and CHX-02 of three cases are compared in Fig. 7. It can be seen from Fig. 7 (a) that temperature differences in CHX-01 of the base case are a little bit smaller than JT-DMR and CT-DMR when the temperature is lower than 0 °C. However, as the temperature raise above 0 °C, the temperature differences of the base case are significantly larger than JT-DMR and CT-DMR. As shown in Fig. 7 (b), the temperature difference in CHX-02 of CT-DMR is the smallest among three cases due to the appropriate mixed refrigerant in cold MR cycle. Thus, adopting TLSO could reduce the temperature difference in CHX-01 and CHX-02 when compare TDCCs of the base case and JT-DMR. Moreover, applying CT to replace JT could further decrease the temperature difference.

In short, the energy consumption is minimized by reducing the CCs gap with a feasible heat exchanger area in the optimization procedure, which indicates that the pinch point shifted toward the hot end of the temperature difference plot in finding the optimal solution. By contrast, the optimizers try to downgrade the light refrigerant in the MR mixture, leading to an increase in the C_3 flow rate and a decrease in the N_2, C_1, and C_2 flow rates.

By contrast, mass entropy generation across CT has contributed to saving more compression energy than those across JT, as illustrated in Table 6. Mass entropy reduction of CT K-8, K-7, and K-6 of CT-DMR are 89.7%, 71.8%, and 81.8% lower than JT valves JTV-1, JTV-2, and JTV-3, respectively, as shown in Table 6. This is because the near isentropic process occurring in the CT reduces entropy generation dramatically. However, the isenthalpic throttling occurred in the J-T valve cannot avoid a large entropy generation.

5.3. Exergy analysis

The SEC of a system is a crucial factor that can be reduced via system exergy analysis. Moreover, the CCs analysis in section 5.2 unveils which part is involved in increasing work loss through LNG heat exchangers rather than whole components. Nevertheless, it offers more information on the distribution of the exergy destruction in each piece of equipment [44]. It figures out system behavior and provides the right move in the process enhancement by the comparative analysis of different refrigeration systems. The general equation is expressed by Eq. (12) [45] as:

$$E = (H - H_0) - T_0(S - S_0) \tag{12}$$

The physical exergy destruction calculation is performed using the equations of each piece of equipment, which are presented in Ref. [46].

For the compression assembly and pumps [47]:

$$Ex_{Des} = \sum[\dot{m}(Ex_{in} - Ex_{out})] + W \tag{13}$$

For the turbines:

$$Ex_{Des} = \sum[\dot{m}(Ex_{in} - Ex_{out})] - W \tag{14}$$

For the LNG cryogenic exchangers [48]:

$$Ex_{Des} = \sum \dot{m}Ex_{in} - \sum \dot{m}Ex_{out} \tag{15}$$

For the interstage coolers and JT valves:

$$Ex_{Des} = \sum[\dot{m}(Ex_{in} - Ex_{out})] \tag{16}$$

For phase separators:

$$Ex_{Des} = \sum \dot{m}_{in}Ex_{in} - (\sum \dot{m}_{liq.}Ex_{liq.} + \sum \dot{m}_{vap.}Ex_{vap.}) \tag{17}$$

The exergy efficiency of the overall process is defined in Eq. (18) as [49]:

$$\eta_{ex} = \frac{Ex_p}{Ex_f} \tag{18}$$

where Ex_p and Ex_f denote the product exergy and fuel exergy, respectively.

Based on the Eqs. (13)–(17), the exergy destruction CT-DMR and JT-DMR compared to the base case was carried out. The results are summarized in Table 7. According to Table 7, the CT-DMR has the lowest net exergy destruction of 17,935.22 kW, which is 40.70% lower than that of the base case. Moreover, the overall exergy destruction of the JT-DMR is 21,958.52 kW, which is 20.74% lower than that of the base case. It indicates that TLSO provides improved mixed refrigerant compositions and operational parameters than KBO because of its superior search capability. Adopting CT in the DMR process shows 18.32% lower exergy destruction than the conventional DMR process, which implies that the CT-DMR leads to the most suitable MR components for the process compared to the base case and the JT-DMR process. The overall exergy destruction of the JT-DMR and CT-DMR cases optimized by TLSO in terms of the complete process, cold, and warm MR, respectively, are demonstrated in Fig. 8. According to Fig. 8, the highest exergy destruction is achieved in the entire process and cold MR section compared to the warm MR section.

Furthermore, a rigorous analysis was performed to determine which equipment is involved in the highest exergy destruction of the CT-DMR case compared to JT-DMR. The result is presented in Fig. 9. For the CT-DMR case, compressors, water coolers, and LNG exchangers contributed

Table 6
Mass entropy reduction/generation (%) across CT of CT-DMR in comparison to across JT of the JT-DMR process.

Units	Mass entropy generation across JT (kJ/kg-°C)			Units	Mass entropy generation across CT (kJ/kg-°C)			Mass entropy reduction $\%_S = \frac{(\Delta_{JT} - \Delta_{CT})*100}{\Delta_{JT}}$
	S_{in}	S_{out}	$\Delta_{JT} = S_{in} - S_{out}$		S_{in}	S_{in}	$\Delta_{CT} = S_{in} - S_{out}$	
JTV-1	3.995	4.083	0.088	**K-6**	1.502	1.503	0.001	80.0
JTV-2	2.033	2.096	0.063	**K-7**	2.114	2.121	0.007	88.9
JTV-3	1.496	1.501	0.005	**K-8**	4.074	4.083	0.009	89.7

Table 7
Exergy destruction Minimization/Maximization of CT-DMR case with compared to JT-DMR case.

Equipment	Exergy Destructions (Ex_{Des})				
	kW		%	kW	%
	Base case	JT-DMR case		CT-DMR case	
Compressors					
K-1	2066.57	1730.53	16.26	1660.73	19.64
K-2	2220.15	1867.42	15.89	1759.98	20.73
K-3	1886.50	1610.59	14.63	1491.75	20.92
K-4	1474.52	1116.09	24.31	936.37	36.50
K-5	1401.97	1191.79	14.99	926.36	33.92
Net exergy Des.	9049.70	7516.41	16.94	6775.19	25.13
Turbines					
K-6	–	–	–	13.73	–
K-7	–	–	–	126.97	–
K-8	–	–	–	93.28	–
Net exergy Des.	–	–	–	233.98	–
Pumps					
P-1	0.00	0.00	–	0.00	–
Net exergy Des.	*0.00*	*0.00*	–	*0.00*	–
Cryogenic LNG exchangers					
CHX-1	3535.78	3488.00	1.35	2047.32	42.10
CHX-2	4975.41	2524.97	49.25	2360.50	52.56
Net exergy Des.	*8511.20*	6012.97	29.35	4407.81	48.21
Water Coolers					
E-1	723.66	535.40	26.01	471.74	34.81
E-2	2005.08	1462.25	27.07	1395.18	30.42
E-3	2264.15	1545.79	31.73	1671.22	26.19
E-4	508.48	829.09	−63.05	615.98	−21.14
E-5	4036.85	1736.08	56.99	2364.13	41.44
Net exergy Des.	9538.22	6108.61	35.96	6518.24	31.66
Phase Separators					
V-1	0.00	0.00	–	0.00	–
Net exergy Des.	*0.00*	*0.00*	–	*0.00*	–
JT Valves					
JTV-1	905.42	905.42	0.00	–	–
JTV-2	1982.62	1299.49	34.46	–	–
JTV-3	259.41	115.61	55.43	–	–
Net exergy Des.	3147.44	2320.52	26.27	–	–
Overall process exergy destruction					
	30246.56	**21958.52**	***27.40***	**17935.22**	***40.70***

37.8%, 36.3%, and 24.6% to the total exergy destruction, respectively. An increase in entropy is always accompanied by heat transfer and compression, which is the main reason for the highest exergy destruction through the compression system (including compressors and water coolers) and LNG cryogenic exchangers. These can be minimized but not eliminated. Moreover, CT account for only 1.3% of the total exergy destruction in the CT-DMR case, while the JT valves account for 10.6% in the JT-DMR case, which shows the benefit of replacing JT valves with CT.

The thermodynamic cycle performance can be evaluated through the exergy efficiency. Higher exergy efficiency leads to lower exergy destruction and vice-versa. Fig. 10 illustrates the exergy efficiency of the base case, JT-DMR, and CT-DMR. The exergy efficiency of the CT-DMR process is the highest (64.68%) among the three cases, which is 13.37% higher than that of the base case. Moreover, the exergy efficiency of the JT-DMR process is 59.21%, which is 7.9% higher than the base case. Undoubtedly, the high exergy efficiency of the JT-DMR and CT-DMR processes is obtained because of the TLSO, which optimizes the MR compositions in the warm and cold MR refrigeration cycle.

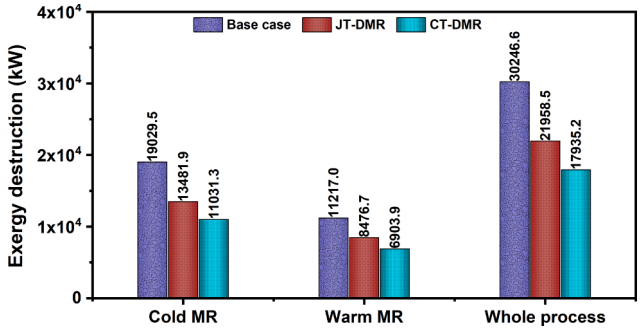

Fig. 8. Overall exergy destruction (kW) of JT-DMR and CT-DMR case optimized by TLSO in comparison to Base case.

Tables 8 and 9 list the coefficient of performance (COP) of each MR cycle and the figure of merit (FOM) of the TLSO-optimized JT-DMR, CT-DMR, and base case, respectively. It can be observed that the JT-DMR and CT-DMR refrigeration cycles have significantly greater overall COP compared to the base case. Moreover, the COP of the overall CT-DMR process, cold MR, and warm MR were 2.42, 1.96, and 3.56, respectively, which are the highest among the three cases. It indicates that the CT-DMR is under the optimal conditions, which is obtained via the TLSO approach that improves the overall COP.

The performance of the liquefaction process can be measured through the FOM with respect to the ideal liquefaction process, as shown in Table 9. A higher FOM indicates the higher performance of liquefaction [50]. Eq. (19) can be used to estimate the FOM.

$$\begin{aligned} &\mathrm{FOM} = \frac{w_{ideal}}{w_{actual}}; \\ &where, \\ &w_{ideal} = \dot{m}_{LNG}[(h_{LNG} - h_0) - T_0(s_{LNG} - s_0)] \end{aligned} \tag{19}$$

where w_{ideal} is the ideal work required for a thermodynamically ideal liquefaction process (at 298.15 K) and w_{actual} is the actual work required for the actual liquefaction process.

The FOM of the CT-DMR is 41.6%, which is 5.2% and 11.9% higher than those of the JT-DMR and the base case, respectively.

6. Conclusions

The dual-mixed refrigerant LNG process has been improved by replacing JT valves with advanced CTs. Replacing an equipment could also lead to non-optimal execution of the entire liquefaction process. Thus, an advanced optimization algorithm, teaching–learning self-study optimization, has been employed to maximize the proposed CT retrofitting performance. The TLSO approach involves a hybrid learning

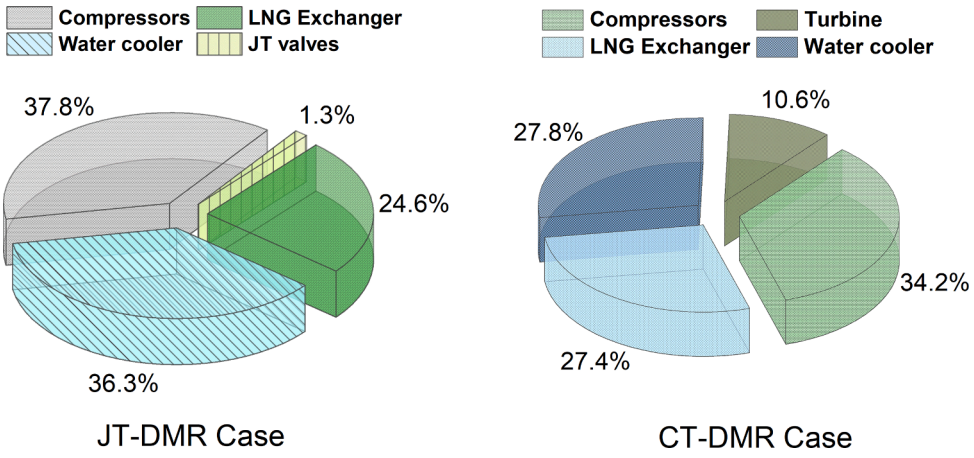

Fig. 9. Exergy contribution rates for TLSO optimized CT-DMR case in comparison to JT-DMR case.

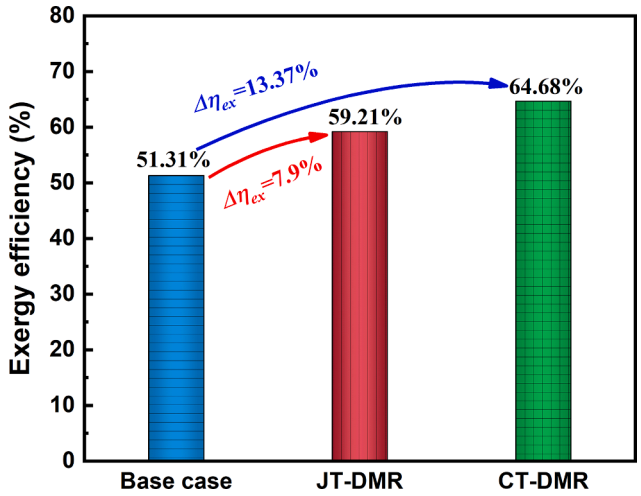

Fig. 10. Exergy efficiency (%) of JT-DMR and CT-DMR case optimized by TLSO in comparison to Base case.

environment (teaching and self-study), which is a natural phenomenon that allows learners to gain knowledge utilizing available resources available such as libraries and academic websites on the internet. This hybrid learning phenomenon makes the TLSO competitive to solve highly non-linear and complex optimization problems with fast convergence and a low probability of getting stuck in local optima. The optimized cryogenic turbine-retrofitted DMR (CT-DMR) process was analyzed by comparing it with the JT valve based DMR (JT-DMR) process. The conclusions are as follows:

- The energy and exergy efficiency of the natural gas liquefaction processes can be improved significantly by replacing isenthalpic expansion device (JT valves) with isentropic expansion device, that is, cryogenic liquid turbine.
- The optimized CT-DMR process can produce LNG with 28.57% less energy consumption compared to the base case.
- The overall exergy destruction of the optimized CT-DMR and JT-DMR was reduced by up to 40.70% and 20.74% compared to the base case, respectively, indicating that TLSO gives promising mixed refrigerant compositions.
- The exergy efficiencies of the optimized CT-DMR and JT-DMR processes are 59.21 and 64.68%, respectively. By contrast, the base case has 51.31% exergy efficiency.

The above analyses confirm that the advanced hydraulic turbine-based DMR can improve the energy efficiency and the refrigeration effect of industrial gas liquefaction processes concerning cohesive energy retrieval.

It is recommended to investigate the energy-saving opportunity of introducing novel refrigerants, i.e. hydrofluoroolefins (HFOs), into the mixed refrigerant and conduct a comprehensive economic analysis and life-cycle assessment on the proposed DMR process in future works. Furthermore, a dynamic study could be beneficial to understand the practical operation characteristic of the CT-DMR process which includes cryogenic turbines.

Table 8
Comparison based on the coefficient of performance (COP) of cold and warm MR.

Decision variables	Coefficient of performance (COP)		
	Base case	JT-DMR	CT-DMR
Cold MR	1.50	1.89	1.96
Warm MR	2.64	3.52	3.56
Overall	1.85	2.38	2.42

Table 9
Figure of Merit comparison between TLSO optimized JT-DMR and CT-DMR case.

Process	Min. Required Work (kW)	Total Energy (kW)	FOM (%)
Base case	12793.0	43039.6	29.7
JT-DMR	12793.0	34751.6	36.8
CT-DMR	12793.0	30725.2	41.6

CRediT authorship contribution statement

Muhammad Abdul Qyyum: Conceptualization, Methodology, Investigation, Software. **Faisal Ahmed:** Methodology, Software. **Alam Nawaz:** Formal analysis, Visualization. **Tianbiao He:** Formal analysis, Writing - original draft, Supervision. **Moonyong Lee:** Supervision, Writing - review & editing, Funding acquisition.

Declaration of Competing Interest

The authors declare that they have no known competing financial interests or personal relationships that could have appeared to influence the work reported in this paper.

Acknowledgments

This research was supported by the Priority Research Centers

Program through the National Research Foundation (NRF) of Korea and funded by the Ministry of Education (2014R1A6A1031189) and the National Natural Science Foundation of China (No. 51906255).

Appendix A. Supplementary data

Supplementary data to this article can be found online at https://doi.org/10.1016/j.apenergy.2021.117187.

References

[1] Qyyum MA, Qadeer K, Lee M. Comprehensive review of the design optimization of natural gas liquefaction processes: Current status and perspectives. Ind Eng Chem Res 2017.
[2] Nguyen T-V, Elmegaard B. Assessment of thermodynamic models for the design, analysis and optimisation of gas liquefaction systems. Appl Energy 2016;183:43–60.
[3] Xiong X, Lin W, Gu A. Design and optimization of offshore natural gas liquefaction processes adopting PLNG (pressurized liquefied natural gas) technology. J Nat Gas Sci Eng 2016;30:379–87.
[4] Mehrpooya M, Ghorbani B. Introducing a hybrid oxy-fuel power generation and natural gas/ carbon dioxide liquefaction process with thermodynamic and economic analysis. J Cleaner Prod 2018;204:1016–33.
[5] Qyyum MA, Chaniago YD, Ali W, Qadeer K, Lee M. Coal to clean energy: Energy-efficient single-loop mixed-refrigerant-based schemes for the liquefaction of synthetic natural gas. J Cleaner Prod 2019;211:574–89.
[6] Nawaz A, Qyyum MA, Qadeer K, Khan MS, Ahmad A, Lee S, et al. Optimization of mixed fluid cascade LNG process using a multivariate Coggins step-up approach: Overall compression power reduction and exergy loss analysis. Int J Refrig 2019;104:189–200.
[7] He T, Liu Z, Ju Y, Parvez AM. A comprehensive optimization and comparison of modified single mixed refrigerant and parallel nitrogen expansion liquefaction process for small-scale mobile LNG plant. Energy 2019;167:1–12.
[8] Khan MS, Lee S, Rangaiah GP, Lee M. Knowledge based decision making method for the selection of mixed refrigerant systems for energy efficient LNG processes. Appl Energy 2013;111:1018–31.
[9] He T, Karimi IA, Ju Y. Review on the Design and Optimization of Natural Gas Liquefaction Processes for Onshore and Offshore Applications. Chem Eng Res Des 2018;132:89–114.
[10] Qyyum MA, Yasin M, Nawaz A, He T, Ali W, Haider J, et al. Single-Solution-Based Vortex Search Strategy for Optimal Design of Offshore and Onshore Natural Gas Liquefaction Processes. Energies. 2020;13:1732.
[11] He T, Mao N, Liu Z, Qyyum MA, Lee M, Pravez AM. Impact of mixed refrigerant selection on energy and exergy performance of natural gas liquefaction processes. Energy 2020;199:117378.
[12] Mortazavi A, Alabdulkarem A, Hwang Y, Radermacher R. Novel combined cycle configurations for propane pre-cooled mixed refrigerant (APCI) natural gas liquefaction cycle. Appl Energy 2014;117:76–86.
[13] Liu Y-N, Newton CL. Feed gas drier precooling in mixed refrigerant natural gas liquefaction processes. Google Patents 1988.
[14] Alabdulkarem A, Mortazavi A, Hwang Y, Radermacher R, Rogers P. Optimization of propane pre-cooled mixed refrigerant LNG plant. Appl Therm Eng 2011;31:1091–8.
[15] Afrand M, Saadat-Targhi M, Khanmohammadi S. Energy and exergy analyses of dual refrigerant system for liquefaction of natural gas. Int J Exergy 2020;31:87–101.
[16] Qyyum MA, He T, Qadeer K, Mao N, Lee S, Lee M. Dual-effect single-mixed refrigeration cycle: An innovative alternative process for energy-efficient and cost-effective natural gas liquefaction. Appl Energy 2020;268:115022.
[17] Vatani A, Mehrpooya M, Palizdar A. Energy and exergy analyses of five conventional liquefied natural gas processes. Int J Energy Res 2014;38:1843–63.
[18] Ma G-g, Zhang C, Ding Y-r, Li B-c. A study on the use of dual mixed refrigerant in a cascade dual mixed refrigerant cycle. Advances in Mechanical Engineering. 2017;9:1–9.
[19] Qyyum MA, Duong PLT, Minh LQ, Lee S, Lee M. Dual mixed refrigerant LNG process: Uncertainty quantification and dimensional reduction sensitivity analysis. Appl Energy 2019;250:1446–56.
[20] Michelsen FA, Halvorsen IJ, Lund BF, Wahl PE. Modeling and simulation for control of the TEALARC liquified natural gas process. Ind Eng Chem Res 2010;49:7389–97.
[21] Husnil YA, Lee M. Synthesis of an Optimizing Control Structure for Dual Mixed Refrigerant Process. J Chem Eng Jpn 2014;47:678–86.
[22] Sun C, Li Y, Zhu J, Han H. Experimental Tube-side Pressure Drop Characteristics of FLNG Spiral Wound Heat Exchanger under Sloshing Conditions. Exp Therm Fluid Sci 2017;88:194–201.
[23] Sun C, Li Y, Han H, Zhu J, Wang S, Liu L. Experimental and numerical simulation study on the offshore adaptability of spiral wound heat exchanger in LNG-FPSO DMR natural gas liquefaction process. Energy 2019;189:116178.
[24] Hwang J-H, Ku N-K, Roh M-I, Lee K-Y. Optimal Design of Liquefaction Cycles of Liquefied Natural Gas Floating, Production, Storage, and Offloading Unit Considering Optimal Synthesis. Ind Eng Chem Res 2013;52:5341–56.
[25] Vatani A, Mehrpooya M, Tirandazi B. A novel process configuration for co-production of NGL and LNG with low energy requirement. Chem Eng Process Process Intensif 2013;63:16–24.
[26] Hwang J-H, Roh M-I, Lee K-Y. Determination of the optimal operating conditions of the dual mixed refrigerant cycle for the LNG FPSO topside liquefaction process. Comput Chem Eng 2013;49:25–36.
[27] Khan MS, Karimi IA, Lee M. Evolution and optimization of the dual mixed refrigerant process of natural gas liquefaction. Appl Therm Eng 2016;96:320–9.
[28] Lee I, Moon I. Economic Optimization of Dual Mixed Refrigerant Liquefied Natural Gas Plant Considering Natural Gas Extraction Rate. Ind Eng Chem Res 2017;56:2804–14.
[29] Vikse M, Watson HA, Kim D, Barton PI, Gundersen T. Optimization of a dual mixed refrigerant process using a nonsmooth approach. Energy 2020;196:116999.
[30] Qyyum MA, Qadeer K, Khan MS, Naqvi M, Rehman A, Wang L, et al. Weed colonization-based performance improvement opportunities in dual-mixed refrigerant natural gas liquefaction process. Energy Sci Eng 2020;9:297–312.
[31] Qyyum MA, Ali W, Long NVD, Khan MS, Lee M. Energy efficiency enhancement of a single mixed refrigerant LNG process using a novel hydraulic turbine. Energy 2018;144:968–76.
[32] Xu X, Liu J, Jiang C, Cao L. The correlation between mixed refrigerant composition and ambient conditions in the PRICO LNG process. Appl Energy 2013;102:1127–36.
[33] Peng D-Y, Robinson DB. A new two-constant equation of state. Ind Eng Chem Fundam 1976;15:59–64.
[34] Barnett W, Chiarella C, Keen S, Marks R. Schnabl H. Complexity and Evolution: Cambridge University Press; 2000.
[35] Fischer M, Leung Y. Geo Computational Modelling Techniques and Applications. Berlin: Springer-Verlag; 2001.
[36] Zhou H, Zheng L, Cen K. Computational intelligence approach for NOx emissions minimization in a coal-fired utility boiler. Energy Convers Manage 2010;51:580–6.
[37] Wang W, Liu X. Melt index prediction by least squares support vector machines with an adaptive mutation fruit fly optimization algorithm. Chemometrics and Intelligent Laboratory Systems. 2015;141:79–87.
[38] Zhang X, Chen X, He Z. An ACO-based algorithm for parameter optimization of support vector machines. Expert Syst Appl 2010;37:6618–28.
[39] Chamkalani A, Zendehboudi S, Bahadori A, Kharrat R, Chamkalani R, James L, et al. Integration of LSSVM technique with PSO to determine asphaltene deposition. J Petrol Sci Eng 2014;124:243–53.
[40] Rao RV, Savsani VJ, Vakharia DP. Teaching–learning-based optimization: A novel method for constrained mechanical design optimization problems. Comput Aided Des 2011;43:303–15.
[41] Li G, Niu P, Zhang W, Liu Y. Model NOx emissions by least squares support vector machine with tuning based on ameliorated teaching–learning-based optimization. Chemometrics and Intelligent Laboratory Systems. 2013;126:11–20.
[42] Ahmed F, Kim J-K, Khan AU, Park HY, Yeo YK. A Fast Converging and Consistent Teaching-Learning-Self-Study Algorithm for Optimization: A Case Study of Tuning of LSSVM Parameters for the Prediction of NOx Emissions from a Tangentially Fired Pulverized Coal Boiler. J Chem Eng Jpn 2017;50:273–90.
[43] Deb K. An efficient constraint handling method for genetic algorithms. Comput Methods Appl Mech Eng 2000;186:311–38.
[44] Ng KC, Shahzad MW, Son HS, Hamed OA. An exergy approach to efficiency evaluation of desalination. Appl Phys Lett 2017;110.
[45] Baccanelli M, Langé S, Rocco MV, Pellegrini LA, Colombo E. Low temperature techniques for natural gas purification and LNG production: An energy and exergy analysis. Appl Energy 2016;180:546–59.
[46] Jamil MA, Goraya TS, Shahzad MW, Zubair SM. Exergoeconomic optimization of a shell-and-tube heat exchanger. Energy Convers Manage 2020;226.
[47] Abdollahi-Demneh F, Moosavian MA, Omidkhah MR, Bahmanyar H. Calculating exergy in flowsheeting simulators: A HYSYS implementation. Energy 2011;36:5320–7.
[48] Long NVD, Pham TN, Bahadori A, Lee M. Novel retrofit designs using a modified coordinate descent methodology for improving energy efficiency of natural gas liquid fractionation process. Journal of Natural Gas Science Engineering. 2016;33:458–68.
[49] Ansarinasab H, Mehrpooya M, Mohammadi A. Advanced exergy and exergoeconomic analyses of a hydrogen liquefaction plant equipped with mixed refrigerant system. J Cleaner Prod 2017;144:248–59.
[50] Mokhatab S, Mak JY, Valappil JV, Wood DA. Handbook of liquefied natural gas. Gulf Professional Publishing; 2013.